Atmos. Chem. Phys., 24, 12495–12507, 2024
https://doi.org/10.5194/acp-24-12495-2024


Atmospheric Chemistry and Physics
Open Access
EGU



# Constraining light dependency in modeled emissions through comparison to observed biogenic volatile organic compound (BVOC) concentrations in a southeastern US forest

**Namrata Shanmukh Panji[1], Deborah F. McGlynn[1], Laura E. R. Barry[2], Todd M. Scanlon[2], Manuel T. Lerdau[2], Sally E. Pusede[2], and Gabriel Isaacman-VanWertz[1]**

[1]Department of Civil and Environmental Engineering, Virginia Tech, Blacksburg, VA 24061, USA
[2]Department of Environmental Sciences, University of Virginia, Charlottesville, VA 22904, USA

**Correspondence:** Namrata Shanmukh Panji (namratapanji@vt.edu) and Gabriel Isaacman-VanWertz (ivw@vt.edu)

Received: 5 June 2024 – Discussion started: 18 June 2024
Revised: 12 September 2024 – Accepted: 17 September 2024 – Published: 12 November 2024

**Abstract.** Climate change will bring about changes in meteorological and ecological factors that are currently used in global-scale models to calculate biogenic emissions. By comparing long-term datasets of biogenic compounds to modeled emissions, this work seeks to improve understanding of these models and their driving factors. We compare speciated biogenic volatile organic compound (BVOC) measurements at the Virginia Forest Research Laboratory located in Fluvanna County, VA, USA, for the year 2020 with emissions estimated by the Model of Emissions of Gases and Aerosols from Nature version 3.2 (MEGANv3.2). The emissions were subjected to oxidation in a 0-D box model (F0AM v4.3) to generate time series of modeled concentrations. We find that default light-dependent fractions (LDFs) in the emissions model do not accurately represent observed temporal variability in regional observations. Some monoterpenes with a default light dependence are better represented using light-independent emissions throughout the year ($LDF_{\alpha\text{-pinene}} = 0$, as opposed to 0.6), while others are best represented using a seasonally or temporally dependent light dependence. For example, limonene has the highest correlation between modeled and measured concentrations using an LDF = 0 for January through April and roughly 0.74–0.97 in the summer months, in contrast to the default value of 0.4. The monoterpenes $\beta$-thujene, sabinene, and $\gamma$-terpinene similarly have an LDF that varies throughout the year, with light-dependent behavior in summer, while camphene and $\alpha$-fenchene follow light-independent behavior throughout the year. Simulations of most compounds are consistently underpredicted in the winter months compared to observed concentrations. In contrast, day-to-day variability in the concentrations during summer months are relatively well captured using the coupled emissions–chemistry model constrained by regional concentrations of $NO_X$ and $O_3$.

## 1 Introduction

Reactive organic gases are released into the atmosphere on the scale of $\sim 935\,\mathrm{Tg\,C\,yr^{-1}}$ (Safieddine et al., 2017) and are a critical area of research due to their role in forming ozone and particulate matter, which in turn has detrimental effects on human health, climate change, and air quality (Ebi and McGregor, 2008). Roughly 90 % of non-methane organic carbon is emitted as biogenic volatile organic compounds (BVOCs) from natural sources (Guenther et al., 1995) such as the regular metabolic processes of vegetation and microbial material (Goldstein and Galbally, 2007). Subsequent photochemistry of these compounds results in the formation of secondary pollutants such as tropospheric ozone and

secondary organic aerosol (SOA) (Atkinson, 2000; Atkinson and Arey, 2003; Guenther et al., 1995). Exposure to tropospheric ozone and SOA can cause short-term effects like eye, nose, and throat irritation and respiratory symptoms. Prolonged exposure may lead to severe issues like increased cancer risk and central nervous system, liver, and kidney damage, particularly in vulnerable populations (Kampa and Castanas, 2008). Apart from their effects on human health, they cause radiative forcing that impacts global temperatures (Myhre et al., 2014).

BVOC emissions are influenced by various environmental factors, including temperature, light, ozone levels, and other meteorological conditions. Higher temperatures often lead to increased BVOC emissions due to enhanced metabolic activity in plants (Dindorf et al., 2006; Rasmussen and Went, 1965), and conversely, BVOC emissions can alleviate temperature stresses (Holopainen, 2004; Holopainen and Gershenzon, 2010). Light availability plays a crucial role in the regulation of emissions, with higher radiation levels stimulating photosynthesis and subsequent BVOC production (Sanadze, 1969; Lerdau and Gray, 2003; Dindorf et al., 2006; Li and Sharkey, 2013). Ozone levels can also influence BVOC emissions, with elevated ozone concentrations exacerbating or inhibiting emission rates depending on duration of exposure (Calfapietra et al., 2013; Lu et al., 2019). However, most studies investigate these effects at the leaf-level or tree-level (Yu and Blande, 2021; Chen et al., 2020; Huang et al., 2018; Kivimäenpää et al., 2016; Helmig et al., 2007), and extrapolation to canopy- or ecosystem-scale impacts can be complex. Furthermore, it can be difficult to decouple multiple competing or complementary effects, such as the chemical destruction of emitted BVOCs by increased ozone masking potential increased emissions or changes in stomatal uptake under differing conditions (Fiscus et al., 2005; Herbinger et al., 2007) impacting both BVOC and ozone emission and uptake (Sadiq et al., 2017; Zheng et al., 2015).

In addition to the sensitivity of BVOC emissions to meteorological conditions, they also exhibit plant species specificity and physiology specificity (Llusia et al., 2008). Hence, BVOCs are emitted at varying rates and composition due to the different plant species available in a forest ecosystem and factors such as their leaf age, plant health, and seasonality. Previously, studies have investigated observed temporal BVOC trends on an ecosystem level (Lindwall et al., 2015; Debevec and Sauvage, 2023), and others have modeled global BVOC emissions (Guenther et al., 2006). Global and/or regional BVOC emissions can be estimated using EPA BEIS (Environmental Protection Agency Biogenic Emissions Inventory System available at https://www.epa.gov/air-emissions-modeling/biogenic-emission-inventory-system-beis, last access: 8 November 2024) and the Model of Emissions of Gases and Aerosols from Nature version 3.2 (MEGANv3.2 available at https://bai.ess.uci.edu/megan/data-and-code/megan32, last access: 8 November 2024). In previous comparisons with short-term observations, MEGAN has been shown to be in good agreement for some compounds and some ecosystems but have discrepancies in other cases (Sindelarova et al., 2014). The model has been shown to overpredict nighttime monoterpene emissions due to combining both light- and temperature-dependent effects to calculate monoterpene emissions (Emmerson et al., 2018; Sindelarova et al., 2014). However, the design of MEGAN to couple with different chemical transport mechanisms has allowed regional and global studies of BVOC concentrations (Situ et al., 2013; Emmerson et al., 2018), secondary organic aerosol formation (Yang et al., 2011), and ozone production (Liu et al., 2018). Seasonal variations in BVOC emissions are sensitive to temperature-dependent factors and leaf area index (Zhang et al., 2021).

Many of the parameters used by default in MEGAN have been estimated as global averages, but variation is possible in these parameters to better reflect local or regional conditions. Of particular interest to this work is the light dependence of monoterpenes. Emmerson et al. (2018) studied the effect of light dependence of monoterpene emissions in MEGAN in southeastern Australia where they concluded that disabling the monoterpene light dependence improved the otherwise underpredicted local monoterpene estimations. Analysis of long-term speciated BVOC concentrations at our research site in a southeastern US forest has shown that some monoterpenes exhibit light-independent behavior despite light-dependent defaults in the model, while others have seasonally dependent light dependence (McGlynn et al., 2023a), which is not a default capability of the model. In this study, we aim to enhance our understanding of BVOC emissions by probing the species-specific temporal variations in light-dependent fractions to better represent the observations at a regional-scale southeastern US forest.

## 2 Methods

### 2.1 Ground-based measurements

#### BVOC concentrations

Mixing ratios of BVOCs were measured at the Virginia Forest Research Laboratory (VFRL) in Palmyra, Virginia (37.9229° N, 78.2739° W), using an automated gas chromatograph with flame ionization detector (GC-FID) system (McGlynn et al., 2023b). The sample is collected 20 m above ground, approximately in the middle of the tree canopy, and passed through a sodium-thiosulfate-infused quartz filter (Pollmann et al., 2005) to scrub for ozone. It is then collected onto a multi-bed adsorbent trap which is thermally desorbed once every hour for analysis by the GC-FID (McGlynn et al., 2021). Further details about the instrumental setup, its calibration, and operation are available in McGlynn et al. (2021) and McGlynn et al. (2023b). Currently, 2 years of BVOC

mixing ratios are available (McGlynn, 2021), but in this study, we focus on measurements made between 1 January and 31 December 2020.

### Meteorological data

Apart from BVOC measurements, this database consists of carbon dioxide mixing ratios (LI-7500; LI-COR, Lincoln, Nebraska), meteorological conditions such as downwelling shortwave radiation (CNR4; Kipp & Zonen, Delft, the Netherlands), temperature and relative humidity (HMP45; Vaisala, Helsinki, Finland), pressure (LI-7500; LI-COR, Lincoln, Nebraska), and wind speed and wind direction (CSAT3; Campbell Scientific, Logan, Utah). The solar radiation measurements are made at a height of 41 m and the other measurements at a height of 35 m from the ground. Further, ecological information of the surrounding forest such as species composition and abundance is available in Chan et al. (2011).

## 2.2 Emissions model

### Overview of approach

BVOC emissions are modeled using MEGAN (Model of Emissions of Gases and Aerosols from Nature), a widely recognized mechanistic model that estimates emissions of BVOCs in the atmosphere originating from terrestrial vegetation (Guenther et al., 2012). Leveraging inputs such as plant species, environmental conditions, and meteorological data, the model predicts BVOC emission rates, allowing us to understand their contributions to atmospheric processes. MEGANv3.2 is used in this work. Fundamentally, MEGAN estimates emissions flux ($F_i$) of chemical species $i$ according to Eq. (1):

$$F_i = \gamma_i \sum \epsilon_{i,j} \chi_j, \quad (1)$$

where $\epsilon_{i,j}$ is the emission factor under standard conditions for vegetation type $j$. $\chi_j$ represents the fractional area of a model grid cell covered with vegetation. The emission activity factor ($\gamma_i$) accounts for the environmental and phenological condition processes controlling emissions such as light ($\gamma_P$), temperature ($\gamma_T$), leaf age ($\gamma_A$), soil moisture ($\gamma_{SM}$), leaf area index (LAI), and $CO_2$ inhibition ($\gamma_{CO_2}$) as shown in Eq. (2).

$$\gamma_i = C_{CE} \mathrm{LAI} \gamma_{P,i} \gamma_{T,i} \gamma_{A,i} \gamma_{SM,i} \gamma_{CO_2,i} \quad (2)$$

Emission activity factors describing light and temperature impacts are divided into light-dependent and light-independent components as

$$\gamma_{P,i} = (1 - \mathrm{LDF}_i) + \mathrm{LDF}_i \gamma_{P\_LDF} \text{ and } \gamma_{T,i} = (1 - \mathrm{LDF}_i)\gamma_{T\_LIF,i} + \mathrm{LDF}_i \gamma_{T\_LDF,i}. \quad (3)$$

In Eq. (3), $\mathrm{LDF}_i$ is the light-dependent fraction for compound $i$; $\gamma_{P\_LDF}$ is the light-dependent activity factor, which is based on measurements for isoprene (Guenther et al., 2006); and $\gamma_{T\_LIF,i}$ and $\gamma_{T\_LDF,i}$ are the light-independent and light-dependent fractions of the temperature activity factor for compound $i$ as described by Guenther et al. (2006).

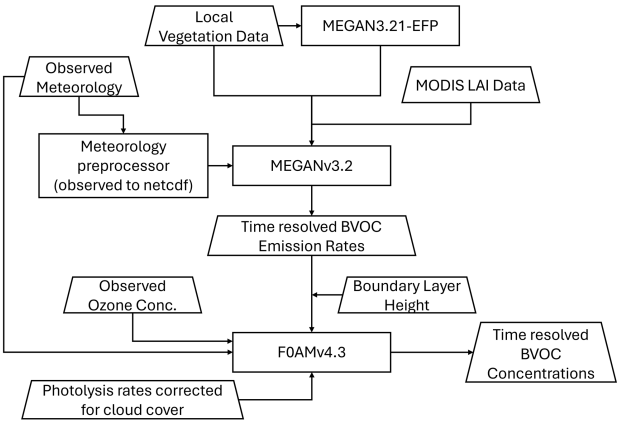


**Figure 1.** Modeling framework used to estimate time-resolved local BVOC concentrations at the Virginia Forest Research Laboratory.

Once BVOCs are emitted into the atmosphere, they undergo photochemical oxidation to produce secondary products. Therefore, to be able to compare our observations of BVOC concentrations with those modeled, we convert the BVOC emission rates estimated by MEGAN to concentrations using a 0-D box model. MEGANv3.2-derived BVOC emissions are provided as inputs to the Framework for 0-D Atmospheric Model (F0AM) box model to simulate photochemistry and estimate time-resolved BVOC concentrations. The framework of this modeling process is shown in Fig. 1.

### MEGANv3.2 parameterization

MEGANv3.2 was run from 2 January to 29 December 2020. A Lambert conformal projection of the United States was used as the grid area for the simulations, where emissions were modeled in the cells encompassing the VFRL site. Emission factors ($\epsilon_{i,j}$) for the VFRL site were calculated using the MEGAN Emission Factor Preprocessor (MEGAN3.21-EFP), available in Python (https://bai.ess.uci.edu/megan/data-and-code/megan32, last access: 8 November 2024), using the tree species composition shown in Table S2 based on a previously reported vegetation survey (Chan et al., 2011); canopy type is 26.88 % needleleaf (predominantly pine) and 73.12 % broadleaf (predominantly oak). The standard condition emission factor for each compound and compound class used in this study have been listed in Table S1 in the Supplement. Leaf area index (LAI) was provided as an input from the Terra MODIS (Moderate Resolution Imaging Spectroradiometer) data product (Myneni et al., 2015), extracted as 8 d averages at the coordinates of the VFRL using the Application for Extracting and Exploring

Analysis Ready Samples (A*pp*EEARS; AppEEARS Team, 2020).

Essential meteorological data required by MEGANv3.2 include temperature, pressure, wind speed, water vapor mixing ratio, and photosynthetically active radiation (PAR). Measurements of relative humidity (%) were converted to water vapor mixing ratio ($kg\,kg^{-1}$) based on temperature and pressure. Downwelling shortwave radiation ($W\,m^{-2}$) measurements were multiplied by 0.5 to convert them to PAR ($W\,m^{-2}$) based on previously reported estimates that half of all incoming radiation is photosynthetically active (McCree, 1981). All meteorological measurements at VFRL were resampled to hourly data and converted to a gridded NetCDF format suitable as input to MEGANv3.2. Gaps in observed meteorological data were filled with measurements from two personal weather stations (Weather Underground identifiers KVATROY19 and KVAPALMY31) located within 2 mi (∼3.2 km) of VFRL as they are highly correlated with observed VFRL data (see Fig. S1 in the Supplement for more information).

A soil type of silty loam was used for the simulations (Soil Survey Staff, Natural Resources Conservation Service, United States Department of Agriculture, 2022). Soil temperature and soil moisture were obtained from the ERA5 (the fifth generation of the European Centre for Medium-Range Weather Forecasts Reanalysis) dataset (Hersbach et al., 2023) using the Open-Meteo API (Zippenfenig, 2023).

Simulations were run at different light-dependent fractions (LDFs) to study the effect of changing emission profiles on diurnal variability in isoprene, $\alpha$-pinene, limonene, and other monoterpenes. A summary of the model cases are listed in Table 1. The LDFs for $\alpha$-pinene and limonene in MEGANv3.2 were changed to the results of positive matrix factorization (PMF) analysis conducted on the annual (September 2019 to September 2020) and summer (June, July, and August 2020) BVOC mixing ratios observed at VFRL (McGlynn et al., 2023a). The resulting time series of emission rates (in $moles\,s^{-1}$) for 200 compounds from MEGANv3.2 were converted to local emission fluxes (in $nmol\,m^{-2}\,s^{-1}$) by dividing emissions by the grid cell area.

### 2.3 F0AM setup

Photochemistry is modeled using the Framework for 0-D Atmospheric Model (F0AM v4.3; Wolfe et al., 2016) 0-D box model that incorporates the Master Chemical Mechanism version 3.3.1 (MCM v3.3.1; MCM, 2024), with a starting point of the sample code "ExampleSetup_DielCycle.m" available with that model. As the VFRL is located in a forest and the closest EPA measurements of $NO_X$ mixing ratios are close to urban cities, $NO_2$ and NO values were constrained to those measured during the 2013 Southern Oxidant and Aerosol Study (SOAS; Southern Oxidant and Aerosol Study, 2013). Because direct measurements of $NO_X$ at the tower were not available, ozone concentrations were constrained by observations rather than produced through photochemistry in the model. Hourly ozone mixing ratios were provided by those obtained from the nearest Environmental Protection Agency (EPA) AirData Air Quality monitors located at Albemarle High School (roughly 15 mi (∼24.1 km) northwest of VFRL) using the Air Quality System (AQS) API v2 (US Environmental Protection Agency, 2024). Since ozone data at this site were only available between March and November 2020, missing values in January through March were filled with those during 2021 from Shenandoah National Park (roughly 41 mi (∼66 km) north of VFRL) and Prince Edward (roughly 53 mi (∼85.3 km) south of VFRL). The diurnal patterns at the Albemarle High School station were similar to those measured at the tower during an overlapping period in 2019, with a bias of 10–20 ppb lower at the EPA station relative to that at the tower (Fig. S5). Because optimum light-dependent factors in this work are determined primarily through correlation and temporal patterns, the similarity in ozone variability between sites does not strongly impact the results of this work, though it does impact model biases (Fig. S6). Further, $H_2$ and $CH_4$ mixing ratios were constrained to 550 and 1770 ppb respectively. Photolysis rates were calculated by the National Center for Atmospheric Research Tropospheric Ultraviolet and Visible (TUV) transfer model (available at https://www2.acom.ucar.edu/modeling/tropospheric-ultraviolet-and-visible-tuv-radiation-model, last access: 8 November 2024) lookup tables as described by Wolfe et al. (2016). As this model estimates photolysis rates under clear cloud conditions, the rates were corrected using the method described by Eq. (4) (Lu et al., 2017).

$$J_{\text{corrected}} = J_{\text{TUV}} \times \frac{\text{SWR}_{\text{cloud}}}{\text{SWR}_{\text{clear}}}, \tag{4}$$

where $J_{\text{corrected}}$ is the corrected photolysis rate, $J_{\text{TUV}}$ is the photolysis rate calculated from the TUV model lookup tables, $\text{SWR}_{\text{cloud}}$ is the observed downwelling shortwave radiation at time $t$ (in $W\,m^{-2}$), and $\text{SWR}_{\text{clear}}$ is the 7 d rolling maximum of the observed downwelling shortwave radiation (in $W\,m^{-2}$) to represent clear-sky conditions. A constant first-order dilution rate of 1 d was used. Observed meteorological data for temperature, pressure, and relative humidity were used. OH concentrations were formed in situ based on photolysis rates and observed concentrations of ozone and water vapor.

To incorporate the emission flux (in $nmol\,m^{-2}\,s^{-1}$) estimated by MEGANv3.2 into the F0AM chemical box model, zero-order reactions were added to the chemical mechanism for each chemical compound, assuming instantaneous emission and mixing into a box whose size was based on the boundary layer height (obtained from Li, 2020). Boundary layer height observations in the Aircraft Meteorological Data Relay (AMDAR) dataset are available regularly but non-continuously throughout the year, and estimation of boundary layer height requires non-trivial data analyses.

**Table 1.** Summary of conditions tested in this study.

| Label | Description | $LDF_{\alpha\text{-pinene}}$ | $LDF_{limonene}$ |
|---|---|---|---|
| Default | LDFs used by default in MEGANv3.2 | 0.6 | 0.4 |
| $PMF_{Annual}$ | Fraction of concentrations attributed to light-dependent factor from a PMF analysis of the annual VFRL dataset* | 0.02 | 0.57 |
| $PMF_{Summer}$ | Fraction of concentrations attributed to light-dependent factor from a PMF analysis of the VFRL summer dataset* | 0.03 | 0.67 |
| $Case_{0.0–1.0}$ | Cases used for correlation studies 1 through 6 | 0, 0.2, 0.4, 0.6, 0.8, 1 | 0, 0.2, 0.4, 0.6, 0.8, 1 |
| Adjusted | Time-dependent LDF based on correlation study | $f_1(t)$ | $f_2(t)$ |

* McGlynn et al. (2023a); $f_1(t)$ and $f_2(t)$ as described in Fig. 6.

Consequently, real-time estimates are not available, and a 7 d rolling average of previously published boundary layer heights for 2007 to 2019 is used (Li, 2020). An average boundary layer height at Dulles International Airport (IAD; near Washington, D.C.) and Raleigh-Durham International Airport (RDU; near Raleigh, NC) are used. Though real-time boundary layer heights for 2020 are reported in the ERA5 dataset, prior work has shown these estimates to be significantly different from observations, so they are not used here (Zhang et al., 2020). The emission rate for F0AM was hence calculated as in Eq. (5):

$$k_{\text{Emission},i}\left(\frac{\text{molecules}}{\text{cm}^3\,\text{s}}\right) = F_i\left(\frac{\text{nmol}}{\text{m}^2\,\text{s}}\right) \times 6.022 \times 10^{23}\left(\frac{\text{molecules}}{\text{mol}}\right) \times 10^{-9}\left(\frac{\text{mol}}{\text{nmol}}\right) \times \frac{1}{\text{BLH (m)}} \times 10^{-6}\left(\frac{\text{m}^3}{\text{cm}^3}\right), \quad (5)$$

where $F_i$ is the emission flux estimated by MEGANv3.2 for compound $i$, and BLH is the boundary layer height (in m). These settings were kept unchanged for all cases listed in Table 1. Results of the F0AM simulations allow us to compare simulated and observed concentrations as reported in the following section.

## 3 Results and discussions

### 3.1 Effect of changing LDF on emissions

Emissions peak during the day, even with relatively high fractions of light-independent emissions (Fig. 2). Overall, light dependence has a stronger impact on nighttime than on daytime concentrations. By decreasing the LDF of $\alpha$-pinene (Fig. 2c) from the default value of 0.6 to nearly 0 (0.02 and 0.03 in annual and summer cases respectively), nighttime emissions increase by 139 %–143 %, and the daytime emissions increase by 47 %–83 %. Similarly, by increasing the LDF of limonene (Fig. 2b) from the default of 0.4 to 0.57 and 0.67 in the annual and summer cases respectively, we see a decrease in the nighttime emissions ranging from 28 %–45 % and daytime emissions from 11 %–29 %. Since the LDF of isoprene was not changed over any of the studies, the estimated emission diurnals remain unchanged (overlapping blue, red, and green lines in Fig. 2) but demonstrate the diurnal profile of a fully light-dependent compound (LDF of 1.0). These effects are observed across all months, though the emission rates in the winter months are approximately 1 %–2 % of those in the summer months. Our observations agree with Emmerson et al. (2018), who note that the nighttime monoterpene emissions in summer increase by 90 %–100 % when LDF is turned off.

Given the impact of LDF on nighttime emissions coupled with the typically low boundary layer height at nighttime (which will present as increased concentrations due to accumulation of emissions), it is important to more closely examine the LDFs that best represent the observed concentrations of various compounds.

### 3.2 Measured vs. modeled BVOC concentrations

Modeled concentrations of monoterpenes generally have maxima in the evening, which agrees with $\alpha$-pinene observations but is in contrast to summertime limonene (Fig. 3). For all monoterpenes, even though observed wintertime concentrations are lower than those in the summer, the model still substantially underestimates concentrations in winter and spring (January to May). Prior studies comparing observed concentrations with those simulated were carried out in peak summer and hence find relatively good agreement (Sindelarova et al., 2014). Concentrations of isoprene were below levels of detection of the GC-FID system through the winter, in contrast to low but non-zero emissions modeled for isoprene. Modeled and observed concentrations in the summer months are comparable in magnitude for all three compounds in the summer, and some day-to-day variability is also captured (Fig. 4). Some day-to-day deviations between modeled and measured concentrations are expected, as

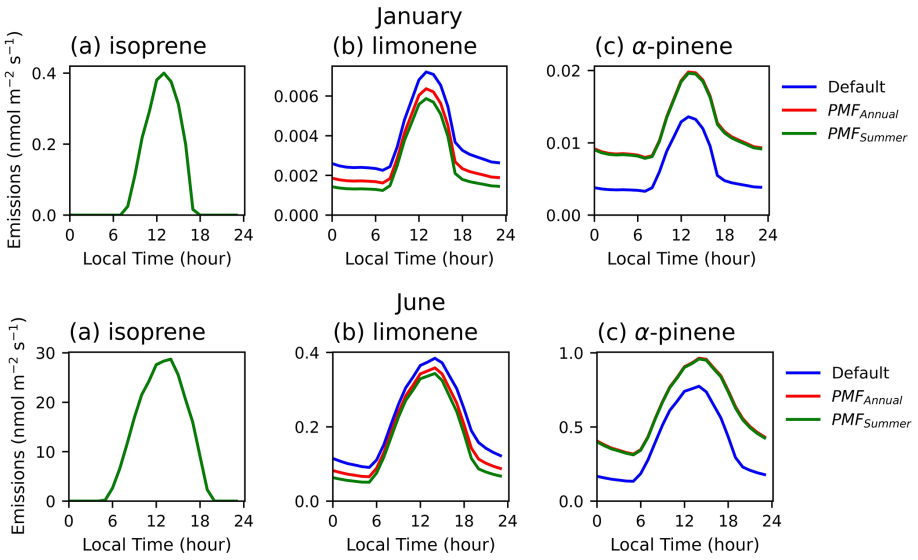


**Figure 2.** Monthly diurnal averages of the **(a)** isoprene, **(b)** limonene, and **(c)** $\alpha$-pinene emissions (in nmol m$^{-2}$ s$^{-1}$) estimated by MEGANv3.2 at VFRL during January (top) and June (bottom) of 2020. The blue, red, and green lines indicate the default ($LDF_{isoprene} = 1$, $LDF_{limonene} = 0.4$, $LDF_{apinene} = 0.6$), $PMF_{Annual}$ ($LDF_{isoprene} = 1$, $LDF_{limonene} = 0.57$, $LDF_{apinene} = 0.03$), and $PMF_{Summer}$ ($LDF_{isoprene} = 1$, $LDF_{limonene} = 0.67$, $LDF_{apinene} = 0.02$) conditions as described in Table 1.

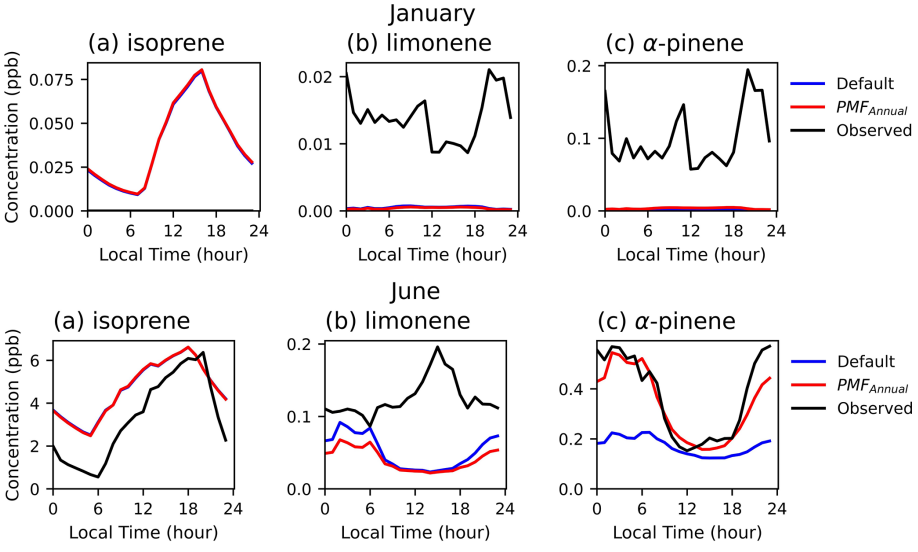


**Figure 3.** Monthly diurnal averages of the **(a)** isoprene, **(b)** limonene, and **(c)** $\alpha$-pinene concentrations (in ppb) estimated by MEGANv3.2 and F0AM at VFRL during January (top) and June (bottom) of 2020. The blue and red lines indicate the default ($LDF_{isoprene} = 1$, $LDF_{limonene} = 0.4$, $LDF_{apinene} = 0.6$) and $PMF_{Annual}$ ($LDF_{isoprene} = 1$, $LDF_{limonene} = 0.57$, $LDF_{apinene} = 0.03$) conditions as described in Table 1, and black lines indicate observed data. Observed concentrations for isoprene were below GC-FID limits of detection for January 2020.

boundary layer heights and some atmospheric composition data are averages, which cannot capture real-world variability. Although there are no isoprene emissions during nighttime (Fig. 2), non-zero nighttime isoprene concentrations are modeled, which may suggest that nighttime chemistry and/or dilution may not be fully captured (Fig. 3).

As noted in McGlynn et al. (2023a), limonene in summer follows daytime peaks in concentration consistent with partially light-dependent behavior and nighttime peaks during winter. The model fails to capture these observed trends, with either default LDF values or those estimated using the fraction of limonene estimated to be light-dependent based on factorization ($\sim 60\,\%$). In contrast, $\alpha$-pinene has nighttime peaks, which are approximately captured by default values and by changing the LDF to 0.03. Importantly, it is clear that the LDF that best captures observed variability may

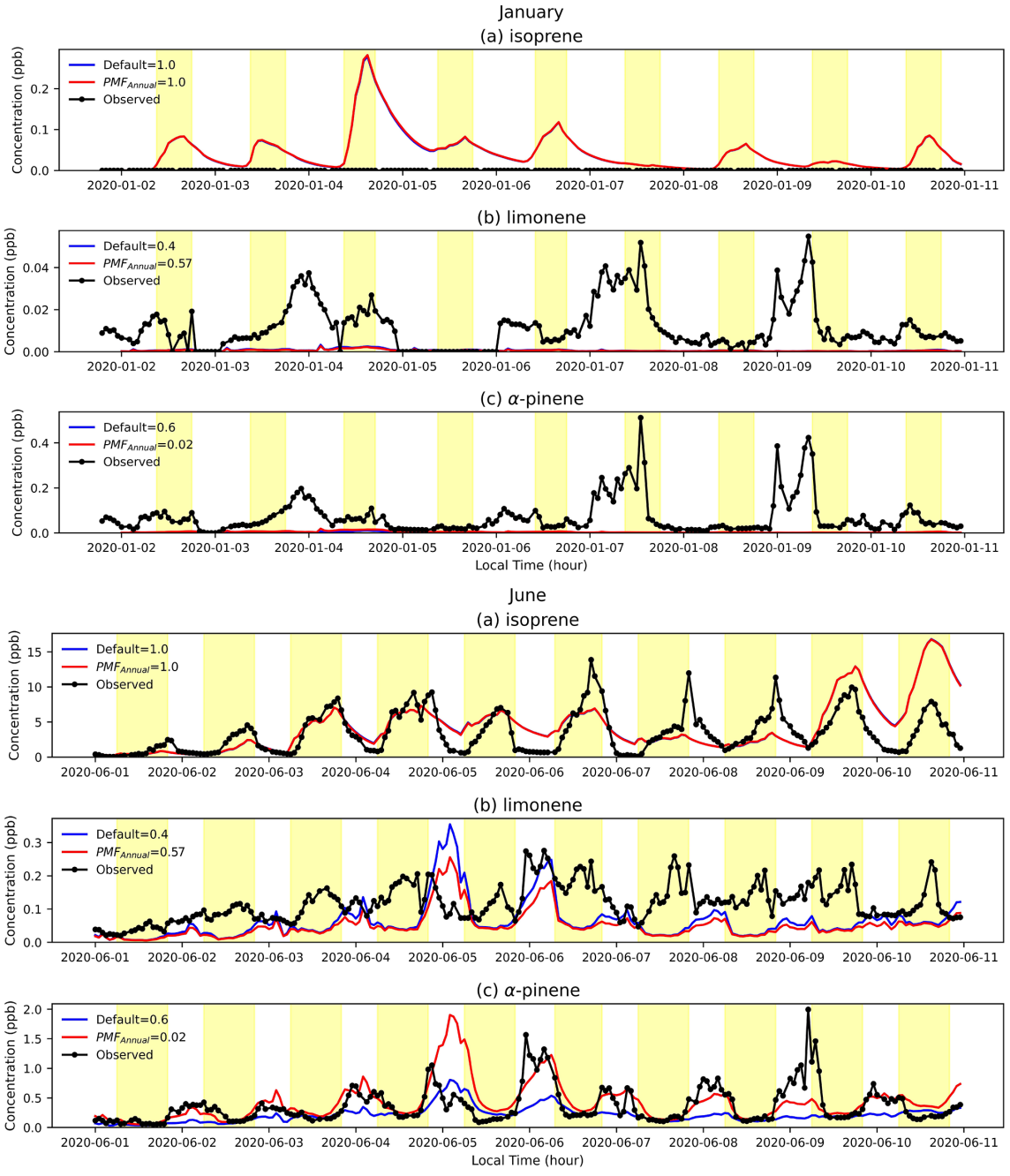


**Figure 4.** A snapshot of concentrations (in ppb) of **(a)** isoprene, **(b)** limonene, and **(c)** $\alpha$-pinene estimated by MEGANv3.2 and F0AM at VFRL during January (top) and June (bottom) of 2020. The blue and red lines indicate the default and $PMF_{Annual}$ conditions as described in Table 1, and black lines indicate observed data. Observed concentrations for isoprene were below GC-FID limits of detection for January 2020.

vary throughout the year, indicating important seasonality. Though both compounds are reacting with oxidants during the day, the stronger light dependence of limonene yields a high daytime and low nighttime source that produces a daytime peak, while $\alpha$-pinene has light-independent emissions at night that accumulate in the lower nighttime boundary layer.

### 3.3 Monthly variation in LDF

To understand the variation in LDF throughout the year, we ran MEGAN simulations at six different values of $LDF_{\alpha\text{-pinene}}$ and $LDF_{limonene}$: 0, 0.2, 0.4, 0.6, 0.8, and 1. Emissions from each scenario were provided to the F0AM model, and a snapshot of the results from July 2020 is shown

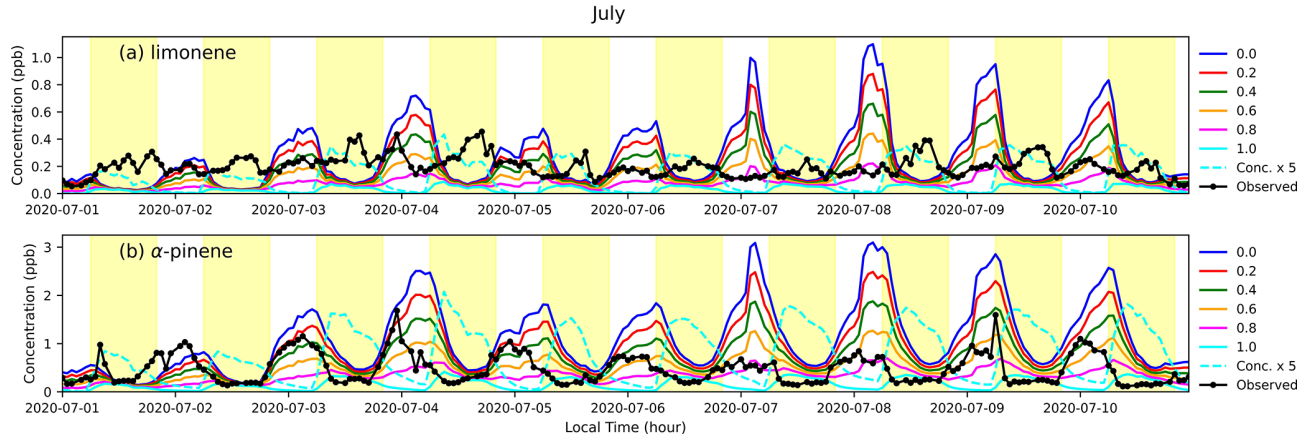


**Figure 5.** A snapshot of **(a)** limonene and **(b)** $\alpha$-pinene concentrations (in ppb) estimated by MEGANv3.2 and F0AM at VFRL during July 2020. The blue, red, green, orange, magenta, and cyan lines refer to simulations with LDF set to 0, 0.2, 0.4, 0.6, 0.8, and 1 respectively (Table 1), and black lines indicate observed data. The dashed cyan line represents the simulated concentrations for LDF = 1.0 multiplied by 5. Daytime hours are highlighted in yellow.

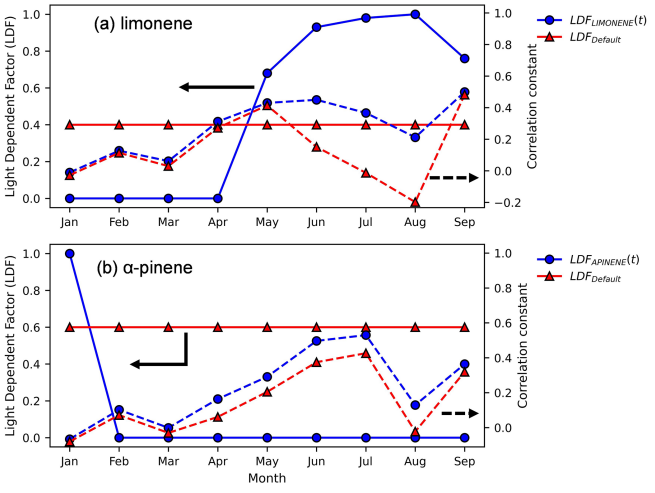


**Figure 6.** Monthly variation in LDF for limonene and $\alpha$-pinene estimated by maximizing the correlation between observed concentrations and those estimated by MEGANv3.2 and F0AM at VFRL. The blue circles and red triangles with solid lines represent the time-dependent and default LDF values respectively, and the dashed lines represent the corresponding Pearson correlation coefficients (axes indicated by black arrows with the same line styles).

in Fig. 5 compared to observed data. As expected from previous studies, concentrations of $\alpha$-pinene correlate well with low values of LDF (Fig. 5b). While low LDF values for limonene better match observations in absolute magnitude, they substantially invert the observed diurnality. Instead, observed concentrations of limonene correlate best with high values of LDF (cyan line in Fig. 5a), though absolute concentrations are underpredicted. To better quantify the monthly variation in LDF with the highest correlation with observed concentrations, the modeled concentrations at the six LDF values (ranging from 0 to 1 as described before) were linearly interpolated in 0.01 increments to achieve a higher resolution. These interpolated concentrations were then compared with observed concentrations to find the LDF that produced the highest correlation. The light dependency of limonene that best correlates with observations varies throughout the year (solid blue line in Fig. 6a), with a peak in light dependence during the summer and less light dependence during the rest of the year. Conversely, a constant $LDF_{\alpha\text{-pinene}}$ of 0 (i.e., light independence) throughout the year slightly improves the correlation coefficient (solid blue line in Fig. 6b).

Simulations were re-run using the LDF value for each month that maximizes correlation (Fig. 7; for $\alpha$-pinene see Fig. S2). In the month of January, there is no discernible increase in correlation by changing the LDF, and the modeled concentrations are extremely low. In the summer (Fig. 7a), the correlation between the simulations and the observed concentrations improves from −0.01 to 0.49 by changing the LDF from a default value of 0.4 to a value of 0.97. However, the magnitude of the modeled concentrations remains low, suggesting underpredicted emission rates and highlighting the significant uncertainty in the understanding of its emissions mechanisms and processes. Notably, the most well-studied compounds, isoprene and $\alpha$-pinene, exhibit more moderate biases, qualitatively supporting the conclusion that the increased study of emissions fluxes from different vegetation under different conditions may improve agreement. In September (Fig. 7b), there is no significant change in the correlation by changing LDF as the diurnal shapes are similar below an LDF of 0.8, but the magnitudes of the concentrations at the adjusted LDFs are closer to those observed.

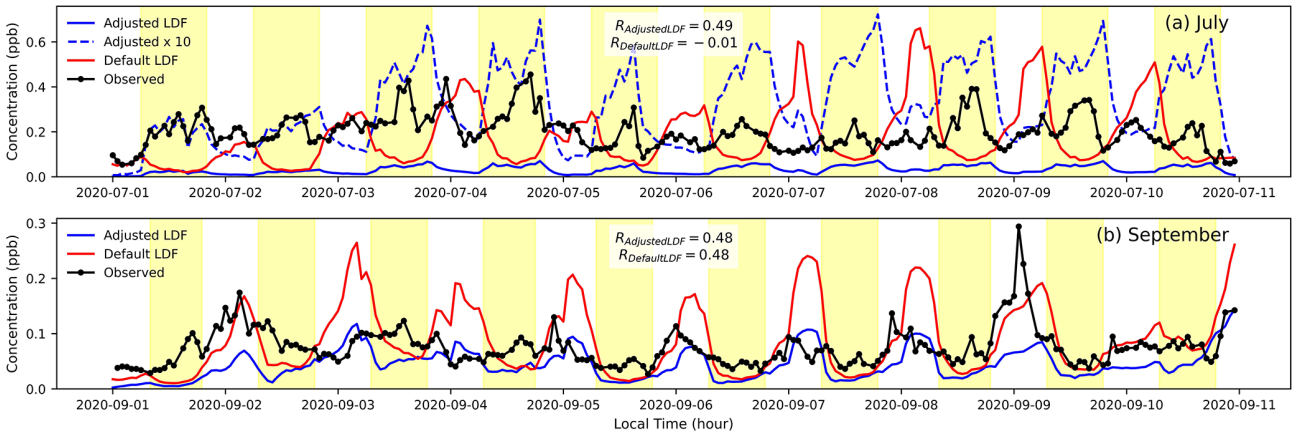


**Figure 7.** A snapshot of limonene concentrations (in ppb) for July and September 2020 using the monthly LDF as shown in Fig. 6. The dashed blue line represents the simulated concentrations for adjusted LDF multiplied by 10. The Pearson correlation coefficient values of the adjusted and default modeled (refer to Table 1) concentrations against the observed concentrations are reported as $R_{\mathrm{AdjustedLDF}}$ and $R_{\mathrm{DefaultLDF}}$.

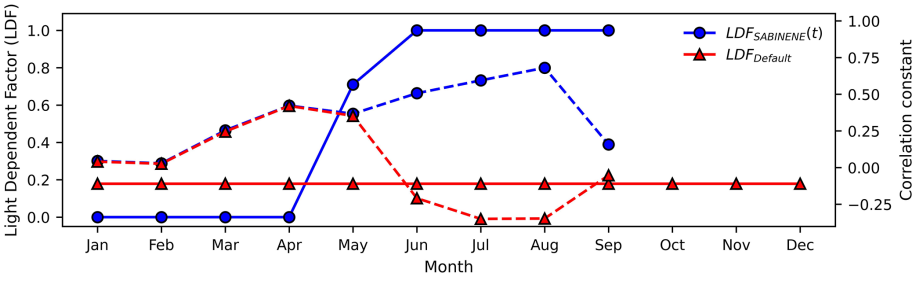


**Figure 8.** Monthly variation in LDF for sabinene estimated by maximizing the correlation between observed concentrations and those estimated by MEGANv3.2 and F0AM at VFRL. The blue circles represent the adjusted LDF values, and the red triangles represent the LDF used by default in MEGANv3.2. The solid blue and red lines represent the LDF values, and the dashed lines represent the corresponding Pearson correlation coefficients.

### 3.4 Extension of F0AM for other BVOCs

Currently, MCM 3.3.1 used during F0AM simulations contains only isoprene and three monoterpenes: $\alpha$-pinene, $\beta$-pinene, and limonene. To simulate the concentrations of other compounds measured at VFRL, we added dummy chemical reactions in the MCM to simulate the chemical loss of other BVOCs emitted into the box for which observational data are available. The reaction rates used are as listed in Table S3.

Following the method described in Sect. 3.3, the monthly variation in sabinene is shown in Fig. 8 and those of $\alpha$-fenchene, $\beta$-phellandrene, $\beta$-thujene, camphene, tricyclene, and $\gamma$-terpinene in Fig. S3. Sabinene is observed to be almost completely light-dependent in the summer, with strong daytime peaks (Figs. 8 and 9). Similarly, variation in LDFs for $\beta$-thujene and $\gamma$-terpinene follows a similar pattern to that of limonene, where the LDF peaks in the summer and falls off during the rest of the year. $\beta$-Phellandrene shows no significant increase in correlation for LDFs between 0–0.8, but the correlation deteriorates to negative values (Fig. S4) if we assume it is completely light-dependent (LDF = 1). By default, MEGANv3.2 assigns the limonene compound class LDF for $\beta$-phellandrene and $\gamma$-terpinene (LDF = 0.4) and carene compound class LDF for sabinene, $\alpha$-fenchene, $\beta$-thujene, camphene, and tricyclene (LDF = 0.2). It is interesting to note that MEGANv3.2 assumes that sabinene, $\beta$-thujene, and $\gamma$-terpinene are partially light-dependent throughout the year despite more appropriate summertime LDFs of around 1. The results in this study corroborate the PMF observations by McGlynn et al. (2023a), who note that $\beta$-thujene, sabinene, $\gamma$-terpinene, and $\beta$-phellandrene display light-dependent behaviors. Further, $\alpha$-fenchene and camphene behave similarly to $\alpha$-pinene in that they remain completely light-independent throughout the year (as opposed to the 0.2 LDF assumed in the MEGAN model). The seasonal variation in the compounds examined in this study are presented in Table S4. The general conclusions that monoterpene isomers exhibit different light dependence than is the default in emission models and that light dependence is seasonally (or otherwise temporally) variable may be applied more broadly or globally.

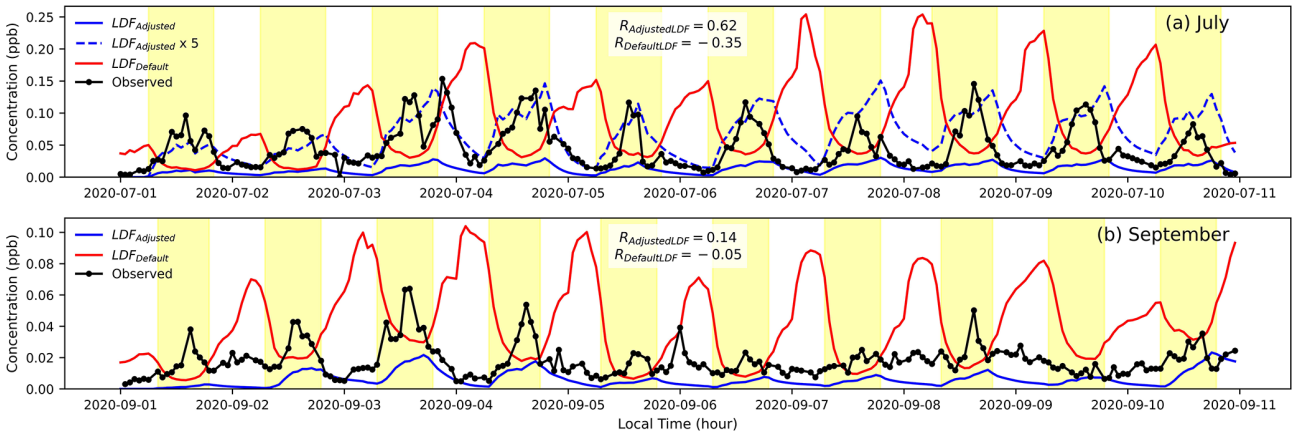


**Figure 9.** A snapshot of sabinene concentrations (in ppb) for July and September of 2020 using the monthly LDF as shown in Fig. 8. The dashed blue line represents the simulated concentrations for adjusted LDF multiplied by 5.

However, we would advise caution in quantitatively applying the values reported here directly to global-scale models without referencing locally observed diurnal patterns as they are likely ecosystem-dependent.

Simulations were run at an LDF of 1 (highest correlation; Fig. 8) for sabinene in July and September. Upon correcting the LDF to be completely light-dependent, sabinene concentrations peak during the daytime to match the diurnals of observed concentrations. Similar to limonene, the magnitudes remain underpredicated. Overall, the variability in LDF throughout the year and the deviation from the values currently used suggest that there is an important seasonality to LDF that needs to be incorporated into emissions models.

## 4 Conclusions

In this study, we used MEGANv3.2 to simulate BVOC emissions during the year 2020 at a southeastern US forest using local ecological and meteorological data. The photochemistry was simulated by F0AM v4.3 to obtain speciated concentration time series. Prior work at this site shows that the LDFs used in these models contradict the light-dependent contribution of some monoterpenes estimated from observed diurnals (McGlynn et al., 2023a). In this work, we demonstrate that LDFs for monoterpenes used by default in the models are not consistent with the observed diurnal and seasonal patterns. We observe an $LDF_{\alpha\text{-pinene}}$ value of 0 (as opposed to 0.6) and a time-dependent $LDF_{\text{limonene}}$ of 0 for January through April and roughly 0.74–0.97 in the summer months, as described in Fig. 6. Further, we were able to extend the model to simulate concentrations of other monoterpenes to get speciated information at our local site. We note that LDFs of the $\alpha$-pinene-like bicyclic monoterpenes camphene and $\alpha$-fenchene follow light-independent behavior throughout the year much like the $\alpha$-pinene. Further, molecules with structures similar to limonene, such as $\beta$-thujene, and bicyclic monoterpenes with a five-carbon ring, such as sabinene and $\gamma$-terpinene, have an LDF that varies throughout the year (like limonene), with light-dependent behavior in summer and light-independent behavior in winter and spring. Lastly, we note that the simulations fail to capture observed concentrations in the winter months where they are consistently underpredicted. The lack of regional $NO_X$ and $O_3$ concentrations, uncertainty in the boundary layer height, and poorly constrained temperature-dependent coefficients and emission factors could be reasons for the discrepancies between the modeled and observed concentrations. Furthermore, intra-annual variability in emission factors (Helmig et al., 2013) and other uncertainty in emissions factors due to a scarcity of temperature- and light-dependent emissions measurements for many of these species could explain seasonal disagreements. Largely, we are able to capture the day-to-day variability in the concentrations during summer months using this relatively simple setup of MEGAN and a 0-D box model with a 7 d rolling average of the boundary layer height conditions and $NO_X$ and $O_3$ concentrations from non-local sources.

This study underscores the need for significant improvements in the LDF within BVOC emission models, particularly for monoterpenes, to more accurately reflect the complex nature of BVOC emissions under varying lighting conditions. The observed seasonality in LDF for specific monoterpenes highlights the importance of incorporating temporal changes into these models. The implications of this research are wide-ranging. Enhancing the precision of BVOC emission models can lead to more accurate forecasts of atmospheric chemistry, which in turn impacts air quality and climate. Improved models will also aid in better understanding the role of BVOCs in the formation of ozone and secondary organic aerosol (SOA), both of which have significant environmental and health impacts. Additionally, acknowledging the seasonality in LDF can guide the develop-

ment of dynamic models that adjust for seasonal variations in monoterpene emissions, thereby increasing the accuracy of emission inventories, especially in regions with pronounced seasonal shifts. Further, the LDF seasonality has important implications for the biology underlying terpene production and emission. Earlier studies have suggested a positive relationship between light dependency and the lack of storage of terpene compounds, e.g., Lerdau and Gray (2003), and the results presented here suggest that metabolic pathways and storage processes may vary both among and within compounds over the course of the year. Compounds showing higher LDFs may be serving as responses to factors that vary with light intensity, so storage is less beneficial, while those with low LDFs are more analogous to constitutive compounds that function in response to factors that act independently of light. Similar results have been shown for certain floral volatiles (Theis et al., 2007), but this study is the first to report such findings for leaf volatiles. Overall, our findings highlight the urgent need for continuous refinement of BVOC emission models. By incorporating more precise LDF parameters and considering seasonal dynamics, we can deepen our comprehension of the interactions between the biosphere and atmosphere, as well as their broader effects on climate and public health.

**Code and data availability.** Data required to run simulations are plotted and provided in Tables S1, S2, and S3. Raw data (i.e., meteorological and BVOC concentrations) are available on request by contacting the corresponding author.

**Supplement.** The supplement related to this article is available online at: https://doi.org/10.5194/acp-24-12495-2024-supplement.

**Author contributions.** NSP: conceptualization, data curation, methodology, investigation, writing (original draft), formal analysis, visualization. GIVW: conceptualization, methodology, writing (review and editing), supervision, funding acquisition. DFM: conceptualization, data curation, writing (review and editing). LERB: writing (review and editing), data curation. TMS: data curation, writing (review and editing). MTL: conceptualization, writing (review and editing). SEP: conceptualization, writing (review and editing), supervision, funding acquisition.

**Competing interests.** The contact author has declared that none of the authors has any competing interests.

**Disclaimer.** Publisher's note: Copernicus Publications remains neutral with regard to jurisdictional claims made in the text, published maps, institutional affiliations, or any other geographical representation in this paper. While Copernicus Publications makes every effort to include appropriate place names, the final responsibility lies with the authors.

**Acknowledgements.** This research was funded by the National Science Foundation (AGS 1837882, AGS 1837891, and AGS 2046367).

**Financial support.** This research has been supported by the National Science Foundation (grant nos. AGS 1837882, AGS 1837891, and AGS 2046367).

**Review statement.** This paper was edited by Kelvin Bates and reviewed by two anonymous referees.

## References

AppEEARS Team: Application for extracting and exploring analysis ready samples (AppEEARS), Sioux Falls, South Dakota, USA: NASA EOSDIS Land Processes Distributed Active Archive Center (LP DAAC), USGS/Earth Resources Observation and Science (EROS) Center, https://appeears.earthdatacloud.nasa.gov/ (last access: 4 July 2023), 2020.

Atkinson, R.: Atmospheric chemistry of VOCs and NOx, Atmos. Environ., 34, 2063–2101, 2000.

Atkinson, R. and Arey, J.: Gas-phase tropospheric chemistry of biogenic volatile organic compounds: a review, Atmos. Environ., 37, 197–219, 2003.

Calfapietra, C., Pallozzi, E., Lusini, I., and Velikova, V.: Modification of BVOC emissions by changes in atmospheric [$CO_2$] and air pollution, Biology, controls and models of tree volatile organic compound emissions, pp. 253–284, https://doi.org/10.1007/978-94-007-6606-8_10, 2013.

Chan, W.-Y. S., Fuentes, J., Lerdau, M., Shugart, H., Scanlon, T., and Clarens, A.: The Fate of Biogenic Hydrocarbons within a Forest Canopy: Field Observation and Model Results, PhD thesis, University of Virginia, https://doi.org/10.18130/V3MV8J, 2011.

Chen, J., Tang, J., and Yu, X.: Environmental and physiological controls on diurnal and seasonal patterns of biogenic volatile organic compound emissions from five dominant woody species under field conditions, Environ. Pollut., 259, 113955, https://doi.org/10.1016/j.envpol.2020.113955, 2020.

Debevec, C. and Sauvage, S.: Temporal and spatial variabilities of volatile organic compounds in the Mediterranean atmosphere, in: Atmospheric Chemistry in the Mediterranean Region: Volume 1-Background Information and Pollutant Distribution, Springer, 505–536, https://doi.org/10.1007/978-3-031-12741-0_15, 2023.

Dindorf, T., Kuhn, U., Ganzeveld, L., Schebeske, G., Ciccioli, P., Holzke, C., Köble, R., Seufert, G., and Kesselmeier, J.: Significant light and temperature dependent monoterpene emissions from European beech (Fagus sylvatica L.) and their potential impact on the European volatile organic compound budget, J. Geophys. Res.-Atmos., 111, https://doi.org/10.1029/2005JD006751, 2006.

Ebi, K. L. and McGregor, G.: Climate change, tropospheric ozone and particulate matter, and health impacts, Environ. Health Persp., 116, 1449–1455, 2008.

Emmerson, K. M., Cope, M. E., Galbally, I. E., Lee, S., and Nelson, P. F.: Isoprene and monoterpene emissions in south-east Australia: comparison of a multi-layer canopy model with MEGAN and with atmospheric observations, Atmos. Chem. Phys., 18, 7539–7556, https://doi.org/10.5194/acp-18-7539-2018, 2018.

Fiscus, E. L., Booker, F. L., and Burkey, K. O.: Crop responses to ozone: uptake, modes of action, carbon assimilation and partitioning, Plant Cell Environ., 28, 997–1011, 2005.

Goldstein, A. H. and Galbally, I. E.: Known and unexplored organic constituents in the earth's atmosphere, Environ. Sci. Technol., 41, 1514–1521, 2007.

Guenther, A., Hewitt, C. N., Erickson, D., Fall, R., Geron, C., Graedel, T., Harley, P., Klinger, L., Lerdau, M., McKay, W., Pierce, T., Scholes, B., Steinbrecher, R., Tallamraju, R., Taylor, J., and Zimmerman, P.: A global model of natural volatile organic compound emissions, J. Geophys. Res.- Atmos., 100, 8873–8892, https://doi.org/10.1029/94JD02950, 1995.

Guenther, A., Karl, T., Harley, P., Wiedinmyer, C., Palmer, P. I., and Geron, C.: Estimates of global terrestrial isoprene emissions using MEGAN (Model of Emissions of Gases and Aerosols from Nature), Atmos. Chem. Phys., 6, 3181–3210, https://doi.org/10.5194/acp-6-3181-2006, 2006.

Guenther, A. B., Jiang, X., Heald, C. L., Sakulyanontvittaya, T., Duhl, T., Emmons, L. K., and Wang, X.: The Model of Emissions of Gases and Aerosols from Nature version 2.1 (MEGAN2.1): an extended and updated framework for modeling biogenic emissions, Geosci. Model Dev., 5, 1471–1492, https://doi.org/10.5194/gmd-5-1471-2012, 2012.

Helmig, D., Ortega, J., Duhl, T., Tanner, D., Guenther, A., Harley, P., Wiedinmyer, C., Milford, J., and Sakulyanontvittaya, T.: Sesquiterpene emissions from pine trees- identifications, emission rates and flux estimates for the contiguous United States, Environ. Sci. Technol., 41, 1545–1553, 2007.

Helmig, D., Daly, R. W., Milford, J., and Guenther, A.: Seasonal trends of biogenic terpene emissions, Chemosphere, 93, 35–46, 2013.

Herbinger, K., Then, C., Haberer, K., Alexou, M., Löw, M., Remele, K., Rennenberg, H., Matyssek, R., Grill, D., Wieser, G., and Tausz, M.: Gas exchange and antioxidative compounds in young beech trees under free-air ozone exposure and comparisons to adult trees, Plant Biol., 9, 288–297, https://doi.org/10.1055/s-2006-924660, 2007.

Hersbach, H., Bell, B., Berrisford, P., Biavati, G., Horányi, A., Muñoz Sabater, J., Nicolas, J., Peubey, C., Radu, R., Rozum, I., Schepers, D., Simmons, A., Soci, C., Dee, D., and Thépaut, J.-N.: ERA5 hourly data on single levels from 1940 to present, Copernicus Climate Change Service (C3S) Climate Data Store (CDS) [dataset], https://doi.org/10.24381/cds.adbb2d47, 2023.

Holopainen, J. K.: Multiple functions of inducible plant volatiles, Trends Plant Sci., 9, 529–533, 2004.

Holopainen, J. K. and Gershenzon, J.: Multiple stress factors and the emission of plant VOCs, Trends Plant Sci., 15, 176–184, 2010.

Huang, J., Hartmann, H., Hellén, H., Wisthaler, A., Perreca, E., Weinhold, A., Ru¨cker, A., van Dam, N. M., Gershenzon, J., Trumbore, S., and Behrendt, T.: New perspectives on $CO_2$, temperature, and light effects on BVOC emissions using online measurements by PTR-MS and cavity ring-down spectroscopy, Environ. Sci. Technol., 52, 13811–13823, 2018.

Kampa, M. and Castanas, E.: Human health effects of air pollution, Environ. Pollut., 151, 362–367, 2008.

Kivimäenpää, M., Ghimire, R. P., Sutinen, S., Häikiö, E., Kasurinen, A., Holopainen, T., and Holopainen, J. K.: Increases in volatile organic compound emissions of Scots pine in response to elevated ozone and warming are modified by herbivory and soil nitrogen availability, Eur. J. Forest Res., 135, 343–360, 2016.

Lerdau, M. and Gray, D.: Ecology and evolution of light-dependent and light-independent phytogenic volatile organic carbon, New Phytol., 157, 199–211, 2003.

Li, D.: AMDAR-BL-PBLH-DATASET, Zenodo [data set], https://doi.org/10.5281/zenodo.3934378, 2020.

Li, Z. and Sharkey, T. D.: Metabolic profiling of the methylerythritol phosphate pathway reveals the source of post-illumination isoprene burst from leaves, Plant Cell Environ., 36, 429–437, 2013.

Lindwall, F., Faubert, P., and Rinnan, R.: Diel variation of biogenic volatile organic compound emissions-a field study in the sub, low and high arctic on the effect of temperature and light, PloS one, 10, e0123610, https://doi.org/10.1371/journal.pone.0123610, 2015.

Liu, Y., Li, L., An, J., Huang, L., Yan, R., Huang, C., Wang, H., Wang, Q., Wang, M., and Zhang, W.: Estimation of biogenic VOC emissions and its impact on ozone formation over the Yangtze River Delta region, China, Atmos. Environ., 186, 113–128, 2018.

Llusia, J., Penuelas, J., Alessio, G. A., and Estiarte, M.: Contrasting species-specific, compound-specific, seasonal, and interannual responses of foliar isoprenoid emissions to experimental drought in a Mediterranean shrubland, Int. J. Plant Sci., 169, 637–645, 2008.

Lu, X., Chen, N., Wang, Y., Cao, W., Zhu, B., Yao, T., Fung, J. C., and Lau, A. K.: Radical budget and ozone chemistry during autumn in the atmosphere of an urban site in central China, J. Geophys. Res.-Atmos., 122, 3672–3685, https://doi.org/10.1002/2016JD025676, 2017.

Lu, X., Zhang, L., and Shen, L.: Meteorology and climate influences on tropospheric ozone: a review of natural sources, chemistry, and transport patterns, Current Pollution Reports, 5, 238–260, 2019.

McCree, K. J.: Photosynthetically active radiation, in: Physiological plant ecology I: Responses to the physical environment, Springer, 41–55, https://doi.org/10.1007/978-3-642-68090-8_3, 1981.

McGlynn, D. F., Barry, L. E. R., Lerdau, M. T., Pusede, S. E., and Isaacman-VanWertz, G.: Measurement report: Variability in the composition of biogenic volatile organic compounds in a Southeastern US forest and their role in atmospheric reactivity, Atmos. Chem. Phys., 21, 15755–15770, https://doi.org/10.5194/acp-21-15755-2021, 2021.

McGlynn, D. F., Frazier, G., Barry, L. E. R., Lerdau, M. T., Pusede, S. E., and Isaacman-VanWertz, G.: Minor contributions of daytime monoterpenes are major contributors to atmospheric reactivity, Biogeosciences, 20, 45–55, https://doi.org/10.5194/bg-20-45-2023, 2023a.

McGlynn, D. F., Panji, N. S., Frazier, G., Bi, C., and Isaacman-VanWertz, G.: An autonomous remotely operated gas chromato-

graph for chemically resolved monitoring of atmospheric volatile organic compounds, Environ. Sci. Atmos., 3, 387–398, 2023b.

McGlynn, D. and Isaacman-VanWertz, G.: In-Canopy Biogenic Volatile Organic Compounds Mixing Ratios at the Virginia Forest Lab, Mendeley Data [dataset], V1, https://doi.org/10.17632/jx3vn5xxcn.1, 2021.

MCM: Master Chemical Mechanism v3.3.1, https://mcm.york.ac.uk/ (last access: 8 November 2024), 2024.

Myhre, G., Shindell, D., Bréon, F., Collins, W., Fuglestvedt, J., Huang, J., Koch, D., Lamarque, J., Lee, D., Mendoza, B., Nakajima, T., Robock, A., Stephens, G., Takemura, T., and Zhang, H.: Anthropogenic and natural radiative forcing, Climate Change 2013-The Physical Science Basis. Contribution of Working Group I to the Fifth Assessment Report of the Intergovernmental Panel on Climate Change, https://doi.org/10.1017/CBO9781107415324, 2014.

Myneni, R., Knyazikhin, Y., and Park, T.: MOD15A2H MODIS/Terra leaf area Index/FPAR 8-Day L4 global 500m SIN grid V006, NASA EOSDIS Land Processes DAAC, https://doi.org/10.5067/MODIS/MOD15A2H.006, 2015.

Pollmann, J., Ortega, J., and Helmig, D.: Analysis of atmospheric sesquiterpenes: Sampling losses and mitigation of ozone interferences, Environ. Sci. Technol., 39, 9620–9629, 2005.

Rasmussen, R. A. and Went, F.: Volatile organic material of plant origin in the atmosphere, P. Natl. Acad. Sci. USA, 53, 215–220, 1965.

Sadiq, M., Tai, A. P. K., Lombardozzi, D., and Val Martin, M.: Effects of ozone–vegetation coupling on surface ozone air quality via biogeochemical and meteorological feedbacks, Atmos. Chem. Phys., 17, 3055–3066, https://doi.org/10.5194/acp-17-3055-2017, 2017.

Safieddine, S. A., Heald, C. L., and Henderson, B. H.: The global nonmethane reactive organic carbon budget: A modeling perspective, Geophys. Res. Lett., 44, 3897–3906, 2017.

Sanadze, G.: Light-dependent excretion of molecular isoprene, Prog. Photosynth. Res., 2, 701–707, 1969.

Sindelarova, K., Granier, C., Bouarar, I., Guenther, A., Tilmes, S., Stavrakou, T., Müller, J.-F., Kuhn, U., Stefani, P., and Knorr, W.: Global data set of biogenic VOC emissions calculated by the MEGAN model over the last 30 years, Atmos. Chem. Phys., 14, 9317–9341, https://doi.org/10.5194/acp-14-9317-2014, 2014.

Situ, S., Guenther, A., Wang, X., Jiang, X., Turnipseed, A., Wu, Z., Bai, J., and Wang, X.: Impacts of seasonal and regional variability in biogenic VOC emissions on surface ozone in the Pearl River delta region, China, Atmos. Chem. Phys., 13, 11803–11817, https://doi.org/10.5194/acp-13-11803-2013, 2013.

Soil Survey Staff, Natural Resources Conservation Service, United States Department of Agriculture: Web Soil Survey, Available online, https://websoilsurvey.nrcs.usda.gov/app/ (last access: 25 January 2024), 2022.

Southern Oxidant and Aerosol Study: Southern Oxidant and Aerosol Study, https://www.eol.ucar.edu/field_projects/sas (last access: 8 November 2024), 2013.

Theis, N., Lerdau, M., and Raguso, R. A.: The challenge of attracting pollinators while evading floral herbivores: patterns of fragrance emission in Cirsium arvense and Cirsium repandum (Asteraceae), Int. J. Plant Sci., 168, 587–601, 2007.

US Environmental Protection Agency: Air Quality System Data Mart, Available online, https://www.epa.gov/outdoor-air-quality-data, last access: 16 February 2024.

Wolfe, G. M., Marvin, M. R., Roberts, S. J., Travis, K. R., and Liao, J.: The Framework for 0-D Atmospheric Modeling (F0AM) v3.1, Geosci. Model Dev., 9, 3309–3319, https://doi.org/10.5194/gmd-9-3309-2016, 2016.

Yang, Q., W. I. Gustafson Jr., Fast, J. D., Wang, H., Easter, R. C., Morrison, H., Lee, Y.-N., Chapman, E. G., Spak, S. N., and Mena-Carrasco, M. A.: Assessing regional scale predictions of aerosols, marine stratocumulus, and their interactions during VOCALS-REx using WRF-Chem, Atmos. Chem. Phys., 11, 11951–11975, https://doi.org/10.5194/acp-11-11951-2011, 2011.

Yu, H. and Blande, J. D.: Diurnal variation in BVOC emission and $CO_2$ gas exchange from above-and below-ground parts of two coniferous species and their responses to elevated $O_3$, Environ. Pollut., 278, 116830, https://doi.org/10.1016/j.envpol.2021.116830, 2021.

Zhang, M., Zhao, C., Yang, Y., Du, Q., Shen, Y., Lin, S., Gu, D., Su, W., and Liu, C.: Modeling sensitivities of BVOCs to different versions of MEGAN emission schemes in WRF-Chem (v3.6) and its impacts over eastern China, Geosci. Model Dev., 14, 6155–6175, https://doi.org/10.5194/gmd-14-6155-2021, 2021.

Zhang, Y., Sun, K., Gao, Z., Pan, Z., Shook, M. A., and Li, D.: Diurnal climatology of planetary boundary layer height over the contiguous United States derived from AMDAR and reanalysis data, J. Geophys. Res.-Atmos., 125, e2020JD032803, https://doi.org/10.1029/2020JD032803, 2020.

Zheng, Y., Unger, N., Barkley, M. P., and Yue, X.: Relationships between photosynthesis and formaldehyde as a probe of isoprene emission, Atmos. Chem. Phys., 15, 8559–8576, https://doi.org/10.5194/acp-15-8559-2015, 2015.

Zippenfenig, P.: Open-Meteo.com Weather API, Zenodo, https://doi.org/10.5281/zenodo.7970649, 2023.